Biointerface Research in Applied Chemistry
Open-Access Journal (ISSN: 2069-5837)

Article
Volume 16, Issue 3, 2026, 96
https://doi.org/10.33263/BRIAC163.096

Synthesis of Hydrotalcite Catalyst and Impregnation with Nickel-Vanadium Metal for the Hydrocracking Process of Waste Cooking Oil to Rich Aromatic Hydrocarbon

Muhammad Al Muttaqii [1,*], Lenny Marlinda [2], Sugeng Priyanto [3], Maja Pranata Marbun [4], Aisha Andini Indira Dewi [2], Sudibyo [5], Abdul Aziz [6], Hendris Hendarsyah Kurniawan [7], Athessia Naomi Nainggolan [8], Hafiizh Prasetia [9], Reva Edra Nugraha [10]

1 Research Center for Catalysis, National Research and Innovation Agency, South Tangerang, Indonesia, 15314; muhammad.al.muttaqii@brin.go.id;
2 Department of Chemistry, Faculty of Science and Technology, University of Jambi, Jambi, 36361 Indonesia; marlindalenny@unja.ac.id;
3 Department of Mechanical Engineering, State University of Jakarta, East Jakarta, 13220, Indonesia; spriyanto@unj.ac.id;
4 Department of Chemical Engineering, Faculty of Engineering, Sunan Bonang University, Tuban, 62314, Indonesia; majapranata123@gmail.com;
5 Research Center for Minerals Technology, National Research and Innovation Agency (BRIN-Indonesia), Lampung Selatan 35361, Indonesia
6 Department of Chemistry, Institut Teknologi Sepuluh Nopember, Keputih, Sukolilo, Surabaya, 60111, Indonesia; azizgb11@gmail.com;
7 Directorate of Laboratory Management, Research, Facilities, and Science and Technology Park - National Research and Innovation Agency (BRIN), Gedung B.J. Habibie, Jalan M.H. Thamrin No. 8, Jakarta Pusat, Indonesia, 10340; hendris.hendarsyah.kurniawan@brin.go.id;
8 Research Center of Materials for Energy - National Research and Innovation Agency, South Tangerang, Indonesia, 15314
9 Research Center for Molecular Chemistry, National Research and Innovation Agency, South Tangerang, Indonesia, 15314; hafiizh.prasetia@gmail.com;
10 Department of Chemical Engineering, Faculty of Engineering, Universitas Pembangunan Nasional "Veteran" Jawa Timur, Surabaya, East Java, 60294, Indonesia; reva.edra.tk@upnjatim.ac.id;
* Correspondence: muhammad.al.muttaqii@brin.go.id;

Received: 13.09.2025; Accepted: 20.05.2026; Published: 15.06.2026

Abstract: Hydrotalcite (HT) was synthesized using a low-supersaturation coprecipitation method from $Mg(NO_3)_2{\cdot}6H_2O$ and $Al(NO_3)_3{\cdot}9H_2O$ precursors (1:1 molar ratio), with Na_2CO_3 as the base and NaOH as the precipitant. The HT material was further modified by loading nickel (Ni) and vanadium (V) metals through a hydrothermal wet impregnation method. X-ray diffraction (XRD) analysis confirmed the successful synthesis of hydrotalcite, showing characteristic diffraction peaks at 2θ values of 11.46°, 23.35°, 34.98°, 39.34°, 47.51°, 60.88°, and 62.13°. Brunauer–Emmett–Teller (BET) analysis revealed a type IV-H3 isotherm with a surface area of 39.99 m^2/g. The best catalytic performance in the hydrocracking of waste cooking oil (WCO) was achieved using the 5% Ni–V (1:2)/HT catalyst. Gas chromatography–mass spectrometry (GC–MS) analysis of the liquid products showed a reduction of carboxylic acids from 94.02% in the feedstock to 19.79%, and increased the hydrocarbon composition reaching 26.69% and aromatic compounds reaching 45.59%. The hydrocarbon product distribution was dominated by the kerosene fraction (C_{10}–C_{13}, 13.72%), followed by gasoil (C_{14}–C_{22}<, 10.22%) and a gasoline fraction (<C_5–C_9, 1.69%), which was not observed with other catalyst modifications.

Keywords: hydrotalcite; nickel-vanadium; hydrocracking; waste cooking oil.

1. Introduction

HT is represented by the formula $Mg_6Al_2(OH)_{16}CO_3{\cdot}4H_2O$, a layered mineral structurally consisting of three layers, namely two outer layers with positive charges (cations) and an inner intermediate layer containing water molecules and anions [1]. Hydrotalcite belongs to the group of layered double hydroxide (LDH) structures or anionic clays with the general structural formula $[M^{2+}_{(1-x)}{\cdot}M^{3+}_x(OH)_2]^{x+}{\cdot}[(A^{n-})_{x/n}{\cdot}yH_2O]^{x-}$, where M^{2+} and M^{3+} are divalent metal cations (such as Mg^{2+}, Ni^{2+}, Zn^{2+}, Cu^{2+}, etc.) and trivalent (such as Al^{3+}, Fe^{3+}, Cr^{3+}, etc.); A^{n-} is an exchangeable interlayer anion; x is the molar ratio of $M^{2+}/(M^{2+} + M^{3+})$ typically found at $0.2 < x < 0.4$ [2]. The special structure of HT results in unique properties, namely good adsorption, tunable surface basicity, large composition variation, homogeneous dispersion of M^{2+} and M^{3+} cations, excellent cation exchange, and also excellent interlayer anions, good thermal stability, and "memory effect" capability [3]. This makes HT compounds promising for applications in adsorption materials, pharmaceuticals, waste treatment, photochemistry, redox reactions, and catalysis [4].

A catalyst is a material used to influence the rate of a chemical reaction due to its ability to lower the activation energy without affecting the equilibrium position of the reaction [5]. Catalysts are generally divided into two categories: homogeneous catalysts, which have the same phase as the reactants (usually liquid or gas), and are composed of only one component. Furthermore, heterogeneous catalysts have a different phase from the reactants and are composed of two or more components (catalyst system: metal and carrier) [6]. Heterogeneous catalysts have advantages over homogeneous catalysts because they are easily separated from the product and can be regenerated, are more economical and environmentally friendly, and are not difficult to dissolve in the reactants [7]. Heterogeneous catalysts are further classified into acidic heterogeneous catalysts (zeolites, non-zeolites, and mesoporous molecular sieves) and basic heterogeneous catalysts (hydrotalcites, oxides, hydroxides, amides, and salts of alkali metals, alkaline earth metals, weak acids, and strong bases) [8].

The preparation method, such as the catalyst, significantly influences its properties by affecting surface area, pH, and metal dispersion within the carrier [9]. Some common methods for producing HT include induced hydrolysis, sol-gel, rehydration/reconstruction, hydrothermal, and coprecipitation at ultra-low saturation while maintaining a constant pH of 7-10 [3]. Coprecipitation is the most widely used method for preparing HT with an interlayer of carbonate anions because it enables large-scale production in a short time by controlling parameters such as metal salt concentration, reagent type, reaction temperature, and washing and drying conditions, as well as pH. Hydrotalcite compounds are highly attractive materials due to their broad applications, economical production, ease of preparation, and the ability to synthesize them with a wide variety of compositions [10]. Hydrotalcite is known as an effective solid base heterogeneous catalyst and is widely used as a catalyst support [11].

A heterogeneous catalyst system consists of a metal-bearing component and a support component [12]. The metal-bearing process on the carrier surface can generally be carried out in three ways, namely dry impregnation, ion exchange, and wet impregnation [13]. This method has the advantage that the metal-bearing phase can be completely dispersed in the carrier, making it more optimal than the other two methods [14]. The wet impregnation method is carried out by wet contact between the catalyst support solid and the metal solution or by immersing the support directly in the metal solution [15]. However, previous studies have reported that bifunctional metal impregnation of the adsorbent material via hydrothermal

treatment significantly increased the specific surface area and pore volume [16]. Similar research was conducted by Madzaki *et al*. [17], who compared hydrothermal impregnation with wet impregnation, showing better material efficiency, increased specific surface area, higher adsorption capacity, and good thermal stability.

Bimetallic heterogeneous catalysts are used in environmental remediation and energy production due to their properties, which can be controlled by the composition of the metal system, the preparation method, and the morphostructure [18]. Nickel (Ni) is a transition metal with catalytic activity comparable to that of noble metals. It is efficient in deoxygenation and hydrotreating reactions. It is more reactive than other transition metals. It is able to accept lone electron pairs, resulting in higher acidity, a property required in cracking reactions. Ni also has a weak bond with the product, making it easily desorbed from the reaction product. However, Ni is susceptible to coke formation and sintering during catalytic deoxygenation reactions. These weaknesses can be overcome by adding promoters such as other transition metals to form bimetallic catalysts [19].

In one period, metals have a tendency to have similar properties, such as metallic properties, magnetism, and reactivity. In the first row of transition metals, there are Scandium (Sc), Titanium (Ti), Vanadium (V), Chromium (Cr), Manganese (Mn), Iron (Fe), Cobalt (Co), Nickel (Ni), Copper (Cu), and Zinc (Zn) [20–23]. Vanadium modification of hydrotalcite shows catalytic activity in oxidative and non-oxidative ethanol dehydrogenation reactions with high conversion. Vanadium/hydrotalcite also reduces the basicity of hydrotalcite [24]. Nazarova *et al*. [25] studied the effect of vanadium-coexisting nickel catalysts on catalytic cracking feedstock. The results showed an increase in the catalyst's dehydrogenation reaction activity, while the reaction with the Ni catalyst alone resulted in increased coking, and the reaction with the V catalyst alone resulted in destructive results with a decrease in catalytic activity, indicated by a decrease in yield percentage. Furthermore, studies of heterogeneous bimetallic Ni-V catalysts supported by hydrotalcite by Costa *et al*. [26] and Summa *et al*. [27], for CO_2 methanation, both showed similar results, where V promotes the texture and electronic properties of Ni/HT. Vanadium changes surface properties, such as surface area and mesoporosity, increases Ni dispersion, affects surface basicity, and increases base sites on the surface. However, the addition of excess V decreases catalytic activity and decreases selectivity. catalyst for methane and promotes the water-gas reverse reaction [28].

The objective of this research is to develop synthesized hydrotalcite catalysts and to modify them through nickel–vanadium metal impregnation, thereby enhancing catalytic activity for the conversion of WCO into liquid biofuels.

2. Materials and Methods

2.1. Materials.

This study were used $Al(NO_3)_3{\cdot}9H_2O$ and $Mg(NO_3)_2{\cdot}6H_2O$ (≥98%, Merck), commercial hydrotalcite (Sigma-Aldrich, with SA=78.0 m^2/g), NaOH (pure pellets, Merck), Na_2CO_3 (≥99.5%, Sigma-Aldrich), HCl (p.a., Merck), Aquades, $Ni(NO_3)_2{\cdot}6H_2O$ (≥99.99%, Merck), V_2O_5 (≥98%, Merck) and Waste Cooking Oil (WCO) was obtained from local market.

2.2. Synthesis of hydrotalcite.

The hydrotalcite synthesis procedure using chemical precursors in this study was carried out using the co-precipitation method (Figure 1), referring to the thesis research of

Hafshah [29] and adapting the research of Arhzaf *et al*. [30]. A precursor solution was prepared, namely a 1:1 mol mixture of $Mg(NO_3)_2 \cdot 6H_2O$ with $Al(NO_3)_3 \cdot 9H_2O$ in 200 mL of distilled water, and a certain amount of base solution was also prepared in the form of 100 mL of 0.5 M Na_2CO_3 and 100 mL of 1.5 M NaOH solution which were added progressively during mixing to maintain the working pH in the range of 10 until a white suspension was formed. Mixing was carried out slowly, with rapid stirring using a magnetic stirrer at 65°C for 5 h, taking care to prevent the sample from evaporating into the environment. After the reaction time was reached, the slurry was aged for 48 h at a temperature of 70°C with slow stirring. The resulting precipitate was vacuum filtered and washed with distilled water until the pH of the wash water was nearly neutral. After that, the resulting precipitate was dried in an oven at 110°C overnight, followed by calcination at 600°C for 6 h and desiccated overnight. Then, samples were prepared for initial characterization and stored in containers labeled "HTs", namely synthetic hydrotalcite.

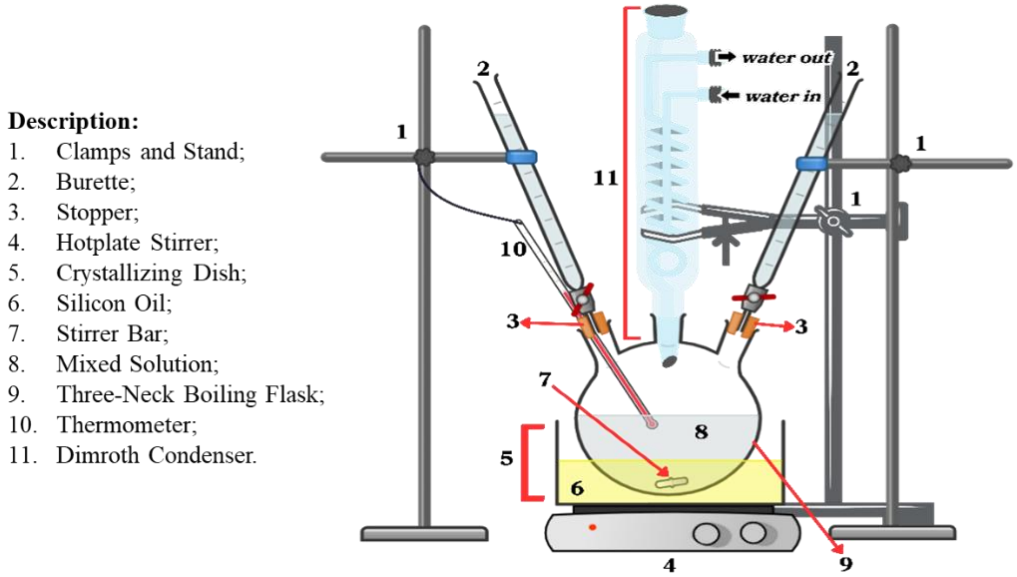

Figure 1. Equipment for hydrotalcite synthesis.

2.3. Impregnation of nickel-vanadium metal in hydrotalcite.

Modification was carried out by adding two metals, Nickel and Vanadium, to the hydrotalcite using a hydrothermal impregnation method. The modification was carried out in stages, using Nickel and then Vanadium, with metal loadings of 5 and 10% and metal ratios of 1:1 and 1:2, resulting in four variations for each type of hydrotalcite. A 10 mL $Ni(NO_3)_2 \cdot 6H_2O$ solution was prepared and then slowly added to the hydrotalcite in a beaker glass with stirring at room temperature for 60 minutes. After that, it was left overnight at room temperature. Next, adapting the research procedure of Utami *et al*. [31], the mixture was put into a hydrothermal vessel and then heated at an oven temperature of 80°C for 4 h. The results obtained were dried at 110°C overnight. Then, with the same steps, this Ni/HT solid was added with 10 mL of V_2O_5 solution in a glass beaker, until finally the NiV/HT solid was obtained. The results were calcined at 550°C for 3 h and then reduced using a hydrogen gas flow at 300°C for 3 h. The results obtained are weighed, stored, and labeled according to the modification conditions and type of support. Then, they were prepared for the characterization stage.

2.4. Catalytic activity.

The catalytic activity testing process in this study was adapted from the methods used by Marlinda *et al*. [20] and Al-Muttaqii *et al*. [32]. The process was carried out using a batch reactor equipped with a mechanical stirrer (Figure 2). A total of 15 mL of WCO (feedstock oil) and 0.5 grams of catalyst were introduced into the reactor. The reactor was then tightly closed to prevent gas from escaping into the environment during the cracking reaction. H_2 gas was breathed into the reactor three times at a pressure of 15-25 bar. Gas was then injected at a pressure of 20 bar with a holding time of approximately 10 minutes to ensure stable pressure. The reaction was carried out for 2 h at 350°C with stirring. After the reaction time was reached, the reactor was allowed to reach room temperature. Next, the product is centrifuged to separate the liquid cracking product and the solid catalyst. The solid catalyst was dried, weighed, the results recorded, and stored with appropriate labels. Then, the liquid product is measured, stored in vials, labeled, and prepared for characterization by GC-MS to determine the composition of the cracking product. The data will be used to analyze the catalytic activity of the catalyst used. The composition of the liquid product (LC) was determined from equation (1) and the Gasoline, Kerosene and Gasoil fractions were determined using equation (2) based on the GC-MS results.

$$\%\text{Yield LC} = \frac{Peak\ area\ of\ compound}{Total\ liquid\ peak\ area}\ x\ 100\% \quad (1)$$

$$\%\text{Yield Fraction} = \frac{Peak\ area\ of\ Fraction}{Total\ hydrocarbon\ peak\ area}\ x\ 100\% \quad (2)$$

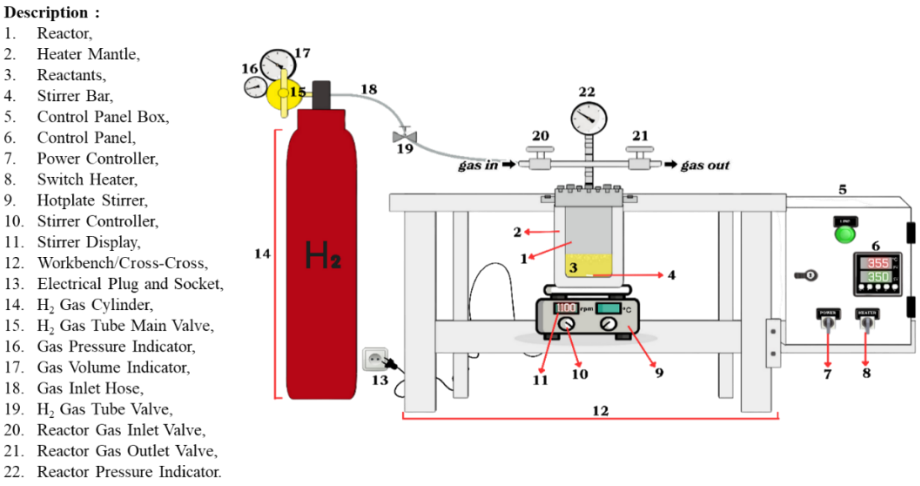

Figure 2. Hydrocracking process equipment.

3. Results and Discussion

3.1. XRD analysis.

In the XRD analysis results for variations of synthesized hydrotalcite, shown in Figure 3. The addition of Nickel and Vanadium metals does not change the structure of the hydrotalcite, but the greater the mass of the added metal, the greater the decrease in the intensity of the diffraction peak in the 2θ = 10-40° region, which indicates a decrease in crystallinity and increases the possibility of a decrease in surface area [33]. Meanwhile, in the 2θ = 35-70° region, there is a shift in the characteristic peak of the hydrotalcite diffractogram [34]. Also, in the 2θ = 35-70°, there is a shift in the characteristic peaks of the hydrotalcite diffractogram,

while the significant difference in the synthesized hydrotalcite is the characteristic peaks of 2θ of Nickel and vanadium metals, which are discussed further in the four modification variations, because the dispersion of the metal at the metal development stage occurs better in the synthesized hydrotalcite. In the 2θ = 37.22° (Ni) and 37.35° (V) regions [35,36], metals were detected with more specific peak intensities than before (JCPDS card No. 89-5144) [37]. Furthermore, at 2θ = 42.29°, a characteristic vanadium peak appeared, which had a higher intensity than the adjacent nickel metal at 2θ = 43.58°; the sharp specific nickel peak in the commercial hydrotalcite modification did not occur. Three characteristic metal peaks were detected in the adjacent 2θ regions, namely 2θ = 61.26 and 65.12° (V) and 63.07° (Ni) (JCPDS No. 18-0888) [38]. According to Paras *et al*. [39], the crystallinity of the material can be determined by the sharpness of the diffraction peaks of the analyzed samples, a broad peak wave indicates an amorphous phase while samples with a high crystalline phase produce very sharp peaks.

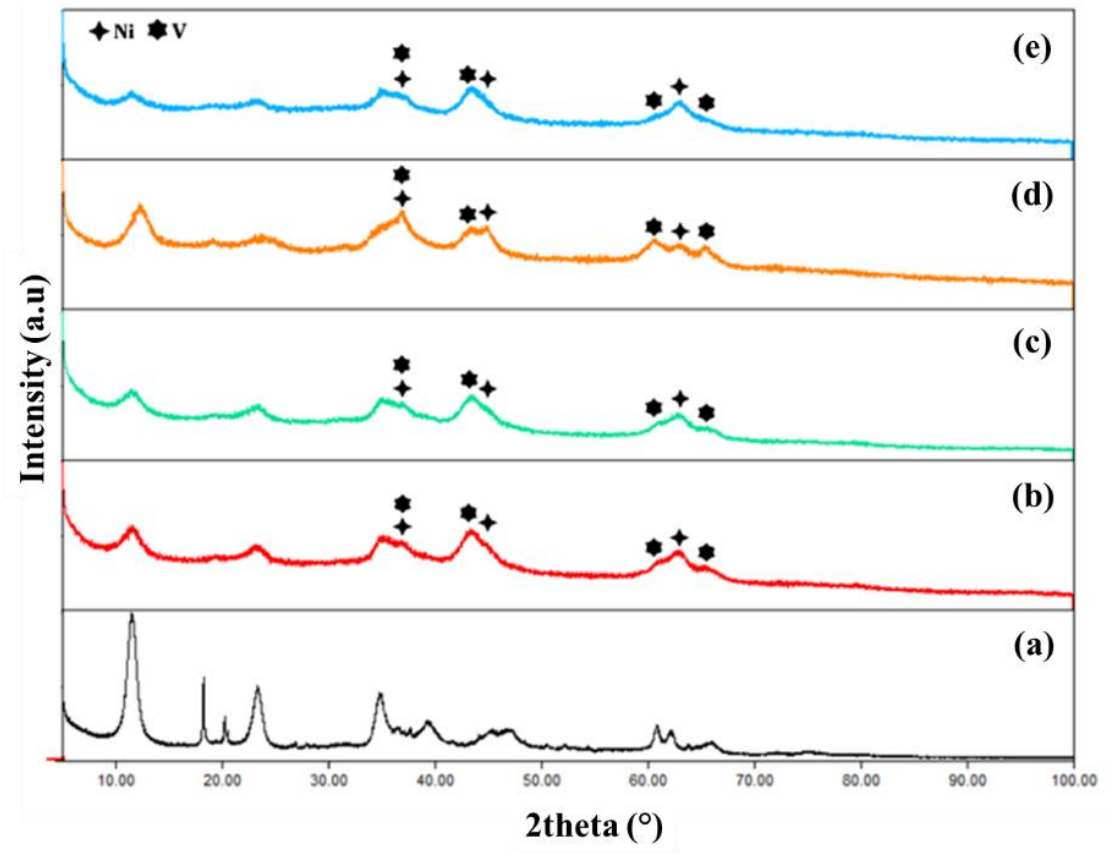

Figure 3. XRD analysis results **(a)** HT; **(b)** 5% Ni-V (1:1)/HTs; **(c)** 5% Ni-V (1:2)/HTs; **(d)** 10% Ni-V (1:1)/HTs; **(e)** 10% Ni-V (1:2)/HTs.

3.2. SEM-EDX analysis.

SEM images were analyzed, and it was seen that the surface shape was almost the same on all catalysts, as shown in Figure 4. The surface of the material formed aggregates that gathered together irregularly. The EDX results show that all hydrotalcite compositions in the material, as well as Ni and V metals, have been successfully impregnated (Figure 5). Mapping of Ni and V metals shows that the metals are evenly distributed on the catalyst surface (Figure 6). Therefore, based on the SEM-EDX results, it shows that Hydrotalcite and Ni-V metal impregnation have been successfully carried out.

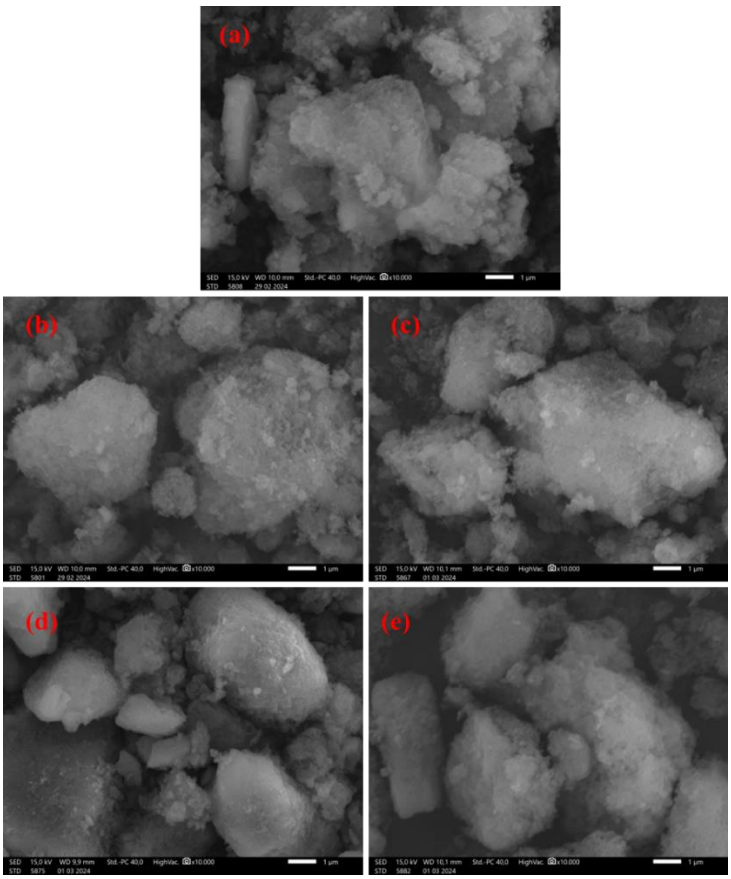

Figure 4. SEM images of **(a)** HTs; **(b)** 5% Ni-V (1:1)/HTs; **(c)** 5% Ni-V (1:2)/HTs; **(d)** 10% Ni-V (1:1)/HTs; **(e)** 10% Ni-V (1:2)/HTs.

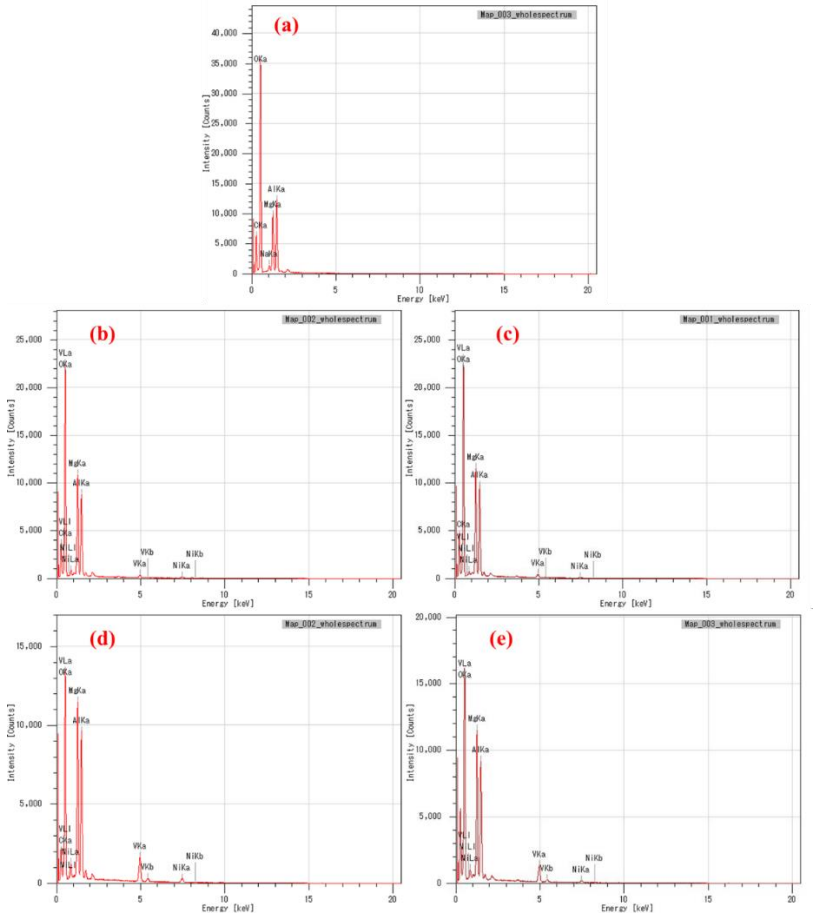

Figure 5. EDX spectra of **(a)** HTs; **(b)** 5% Ni-V (1:1)/HTs; **(c)** 5% Ni-V (1:2)/HTs; **(d)** 10% Ni-V (1:1)/HTs; **(e)** 10% Ni-V (1:2)/HTs.

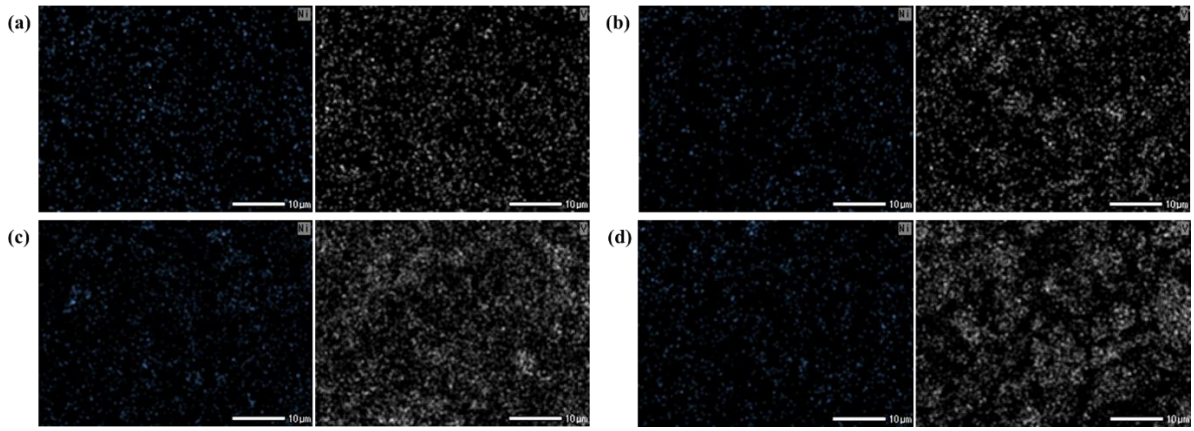

Figure 6. Ni and V Mapping of **(a)** 5% Ni-V (1:1)/HTs**; (b)** 5% Ni-V (1:2)/HTs; **(c)** 10% Ni-V (1:1)/HTs; **(d)** 10% Ni-V (1:2)/HTs.

3.3. N_2 adsorption-desorption analysis.

The synthetic hydrotalcite was analyzed using BET to provide surface character information, in the form of average pore size, total pore volume, and pore distribution data or specific surface area (S_{BET}) [40]. Based on Table 1, the surface area data of the synthetic hydrotalcite is approximately 39.99 m^2/g. The surface area is not larger than the results in the study of Park *et al*. [41]. This discrepancy can occur due to differences in measurement consistency, such as testing conditions, software and tool versions, and sample condition [42].

Based on the data in Table 1, it can be seen that synthetic hydrotalcites have mesoporous particle sizes according to the International Union of Pure and Applied Chemistry (IUPAC) standards, with an average pore diameter of 2-50 nm [43]. Furthermore, in Figure 5, the convex shape of the BET model graph of the N_2 adsorption-desorption isotherm (P/P_0 = 0-1.0) demonstrates that both commercial and synthetic hydrotalcites fall into the type IV adsorption isotherm, indicating a mesoporous structure [44]. The adsorption-desorption isotherm curves exhibit hysteresis loops at high relative pressures, but the desorption lines vary, indicating differences in the type and shape of the hysteresis loops associated with specific pore structures [45]. According to Mališová *et al*. [40], the mesoporous texture of the sample can be seen based on the shape of the curve due to capillary condensation, which forms a hysteresis loop caused by the mechanism of pore filling and emptying under varying material conditions. Furthermore, in the modification of commercial hydrotalcite, the results obtained were comparable to the volumetric, namely the largest increase in surface area was shown in the variation of 5% Ni-V (1:2)/HTs with a surface area of 59.57 m^2/g. A significant decrease in surface area was shown in the variation of 10% Ni-V (1:1)/HTs, namely 11.191 m^2/g. The results of the modification of the synthesized hydrotalcite included mesoporous, with an average diameter in the interval of 25.64-31.22 nm. Based on the research of Pan *et al*. [46], the shape of the N_2 adsorption-desorption isotherm graph on all modifications of commercial hydrotalcite type IV which is included in the classification of hysteresis loops H3 which represents the shape of slit-shaped pores, but in the variation of 10% Ni-V (1:1)/HTs (Figure 7) shows the character of the classification of hysteresis loops H2 which represents the shape of ink bottle pores.

Table 1. BET analysis results of synthetic hydrotalcite and Ni-V/HTS catalysts

Catalysts	Surface area (m^2/g)	Total pore volume (cm^3/g)	D_{pore} (nm)	Metal loading (w.t%)	
				Ni	V
HT	39.99	0.39	39.23	-	-
5% Ni-V (1:1)/HTs	50.14	0.34	27.36	3.49	4.23
5% Ni-V (1:2)/HTs	59.57	0.38	25.64	1.23	1.81

Catalysts	Surface area (m^2/g)	Total pore volume (cm^3/g)	D_{pore} (nm)	Metal loading (w.t%)	
				Ni	V
10% Ni-V (1:1)/HTs	11.19	0.08	31.22	5.20	8.86
10% Ni-V (1:2)/HTs	37.05	0.23	27.36	3.21	9.76

Figure 7 shows the N_2 adsorption-desorption isotherm graph and pore size distribution: a) synthetic hydrotalcite (HTs); b) synthetic hydrotalcite (HTs) and modified synthetic hydrotalcite (HTs) with metal Ni-V: b) 5% (1:1); c) 5% (1:2); d) 10% (1:1); e) 10% (1:2). The synthesized hydrotalcite (Figure 4a) are classified as having H3 hysteresis loops, representing the lamellar slit pore shape. Similar studies that synthesized and characterized materials resembling hydrotalcite or the LDH group found the same isotherm classification, namely the type IV N_2 adsorption-desorption isotherm with H3 hysteresis loops [47,48]. A Barrett-Joyner-Halenda (BJH) adsorption model curve was plotted to obtain the pore size distribution using pore diameter and differential pore volume data [46]. The N2 adsorption-desorption isotherm for all modifications of the synthesized hydrotalcite type IV, which is classified as H3 in the hysteresis loop classification, exhibits a slit-shaped pore structure.

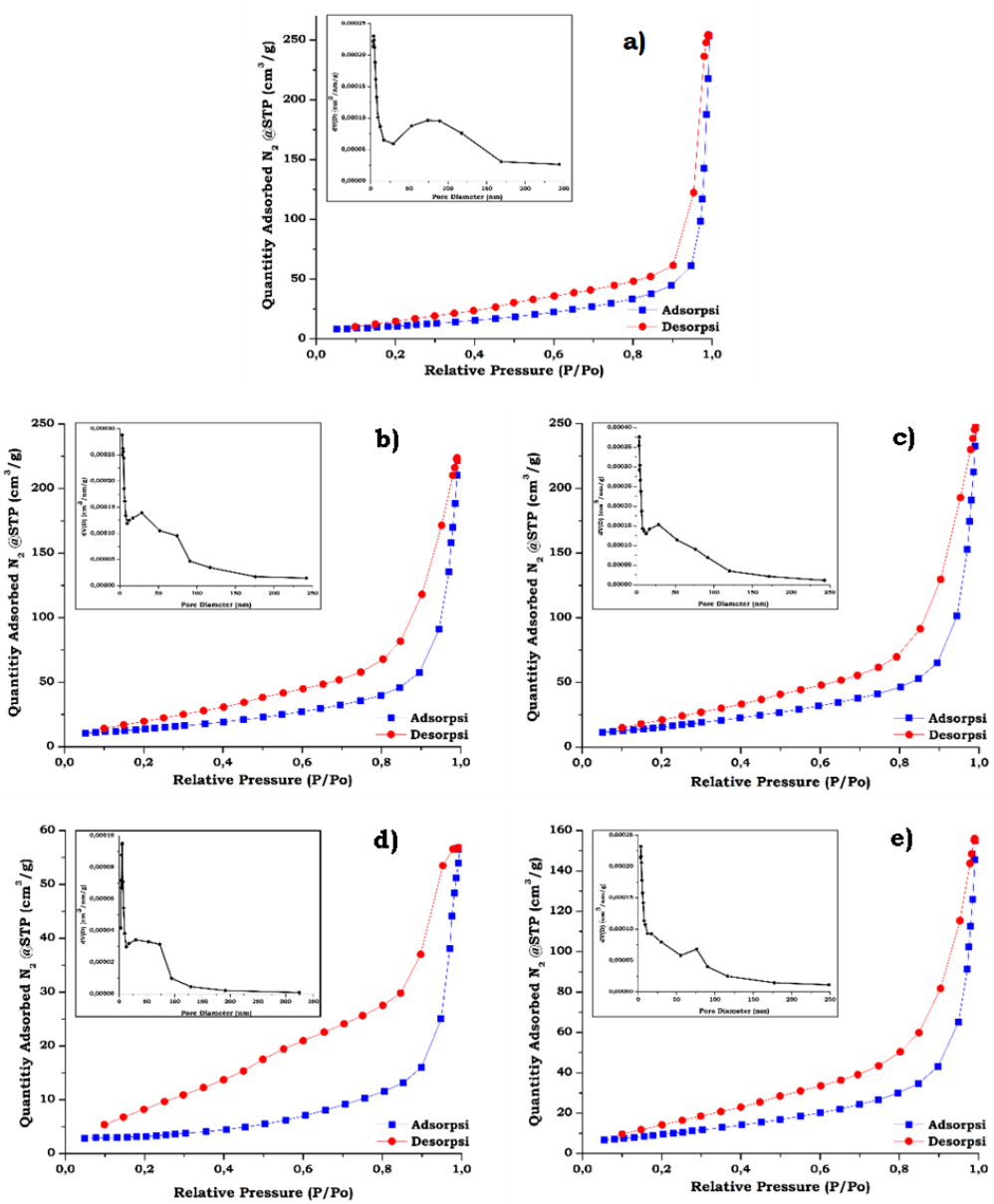

Figure 7. N_2 adsorption-desorption isotherm graph and pore size distribution (Inset) of**(a)** HTs; b)5% Ni-V (1:1)/HTs c) 5% Ni-V (1:2),/HTs d) 10% Ni-V (1:1)/HTs; e) 10% Ni-V (1:2)/HTs

3.4. Catalytic activity.

The modified hydrotalcite was tested for its activity as a catalyst through a hydrogen-pressure cracking reaction, also known as hydrocracking. The feedstock oil used in this study was purified WCO. WCO has significant potential as an alternative raw material for biodiesel fuel conversion due to its high fatty acid content, predominantly oleic and palmitic acids, as shown in Figure 8 [49]. The results of the GC-MS analysis are interpreted in Table 2. The main components in WCO are Dodecanoic acid (30.71 %), Myristic acid (9.95 %), Palmitic acid (19.80 %), (E)-11-Octadecenoic acid (13.72 %), (E)-9-Octadecenoic acid (5.63 %).

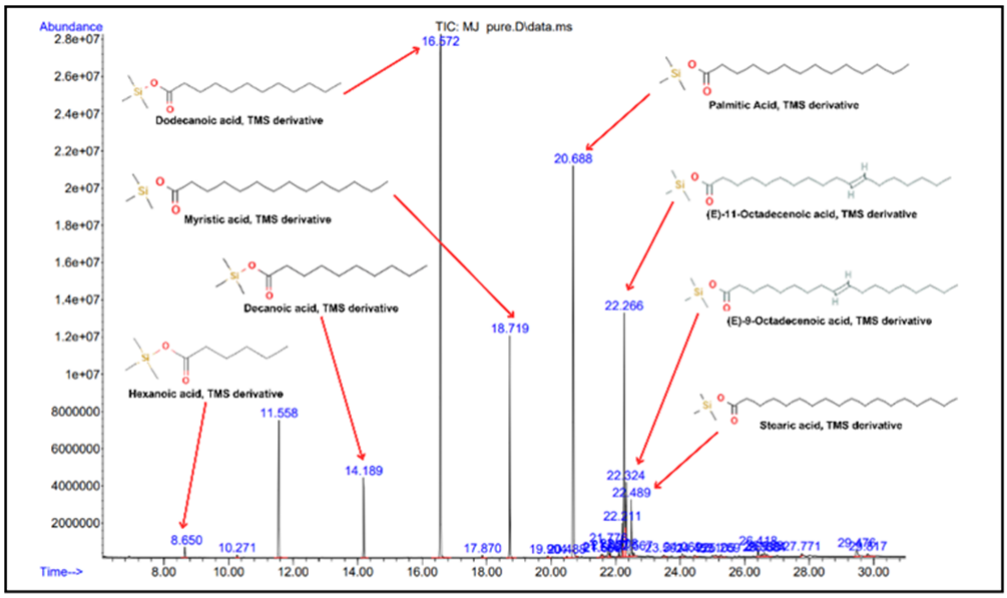

Figure 8. GC-MS chromatogram of purified WCO.

Table 2. The composition of purified used cooking oil.

Compounds	Selectivity (%)
Carboxylic acid	
Hexanoic acid	0.45
6-Methylheptanoic acid	4.67
Decanoic acid	4.19
Dodecanoic acid	30.71
Myristic acid	9.95
Palmitelaidic acid	0.14
Palmitic acid	19.80
cis-Vaccenic acid	0.22
(Z,Z)-9,12-Octadecadienoic acid	1.51
(E)-11-Octadecenoic acid	13.72
(E)-9-Octadecenoic acid	5.63
Stearic acid	2.85
(Z)-Oleic acid	0.18
Ester	2.35
Alcohol	0.92

The liquid product was measured, stored in vials, labeled, and prepared for characterization using GC-MS. The purpose of the analysis was to determine the composition of the cracking product, which would be used to assess the potential catalytic activity of the material used based on its conversion success. In this study, the hydrocracking reaction products were grouped into alkanes (paraffins, isoparaffins, cycloparaffins), alkenes/olefins, monocyclic aromatics, polycyclic aromatics (PAHs), carboxylic acids, esters, alcohols, and other compounds such as ketones, ethers, and amides, as presented in Table 3.

Table 3. Composition of the hydrocarbon compound group of liquid products

Hydrocarbon composition	Catalysts (%)				
	HTs	5% Ni-V (1:1)/HTS	5% Ni-V (1:2)/HTS	10% Ni-V (1:1)/HTS	10% Ni-V (1:2)/HTS
n-Paraffin	1.16	1.40	19.95	1.48	1.69
Iso-paraffin	0.00	0.05	0.44	0,.46	0.00
Cyclo-paraffin	0.89	0.72	4.41	1.66	0.78
Aromatic	0.00	0.00	26.85	0.60	0.04
Olefin	2.51	3.91	1.89	8.89	4.24
Ester, Alcohol	2.27	3.22	0.00	6.01	2.55
PAH	-	-	18.74	-	-
Carboxylic acid	88.71	86.98	19.79	71.58	87.04
Etc.	4.46	3.72	7.93	9.31	3.67

The distribution of compound components resulting from the hydrocracking reaction with synthesized hydrotalcite is shown in Figure 9. The catalytic performance of synthesized hydrotalcite and its Ni–V modified derivatives demonstrated a strong dependence on both catalyst composition and reaction temperature. The unmodified hydrotalcite exhibited poor activity, with 88.71% of carboxylic acids remaining unconverted and only minor formation of alkanes (2.05%) and alkenes (2.51%). Incorporation of Ni and V metals enhanced catalytic activity, as observed with 5% Ni–V at a 1:1 ratio, which slightly increased alkane and alkene yields. A significant improvement was achieved with 5% Ni–V at a 1:2 ratio, where only 19.79% of carboxylic acids remained, and substantial production of alkanes (24.81%), aromatic hydrocarbons (26.65%), and polycyclic aromatic hydrocarbons (18.74%) was obtained. This indicates that the synergistic interaction between Ni (hydrogenation function) and V (redox function) promoted more effective cracking and deoxygenation [50]. However, the high yield of aromatics and PAHs suggests that elevated reaction temperatures favored aromatization and condensation pathways [51]. The formation of aromatic hydrocarbons in hydrocracking reactions affects biofuel quality and catalyst stability. High aromatic content generally lowers the H:C ratio compared to paraffinic hydrocarbons, which can reduce cetane value and result in less clean combustion [52]. Aromatic hydrocarbons can undergo further condensation reactions to form PAHs, which become precursors for coke formation on the catalyst surface. This coke deposition will cover the active sites of the catalyst, both metal and acid sites, and inhibit the diffusion of reactants into the catalyst pores, thus causing a decrease in catalytic activity during the reaction. Therefore, aromatic formation in the hydrocracking process is generally kept to a minimum to meet the desired target fuel requirements, thereby maintaining the quality of the biofuel produced while extending the catalyst's service life [53]. A simple mechanism that could possibly occur is shown in Figure 10. The increase in aromatic products can be caused by the increase in catalyst acidity and the length of time the feedstock is attached to the active site [54]. In contrast, higher metal loading (10% Ni–V at both 1:1 and 1:2 ratios) resulted in decreased activity, with more than 70% of carboxylic acids remaining unconverted. This decline is attributed to metal overloading, which likely blocked active sites and restricted reactant diffusion [55]. Overall, moderate Ni–V loading (5% at 1:2) provided the highest conversion efficiency, while reaction temperature played a critical role in determining product selectivity, where moderate temperatures favored alkane formation, and higher temperatures promoted aromatics and PAHs [56].

In this study, the alkane compounds, namely n-paraffin, isoparaffin, and cycloparaffin, produced by the hydrocracking reaction, were classified into three fractions. These three

fractions are saturated hydrocarbons grouped based on the number of carbon atoms: gasoline (<C_5-C_9), kerosene (C_{10}-C_{13}), and gasoil (C_{14}-C_{22}<), as presented in Table 4.

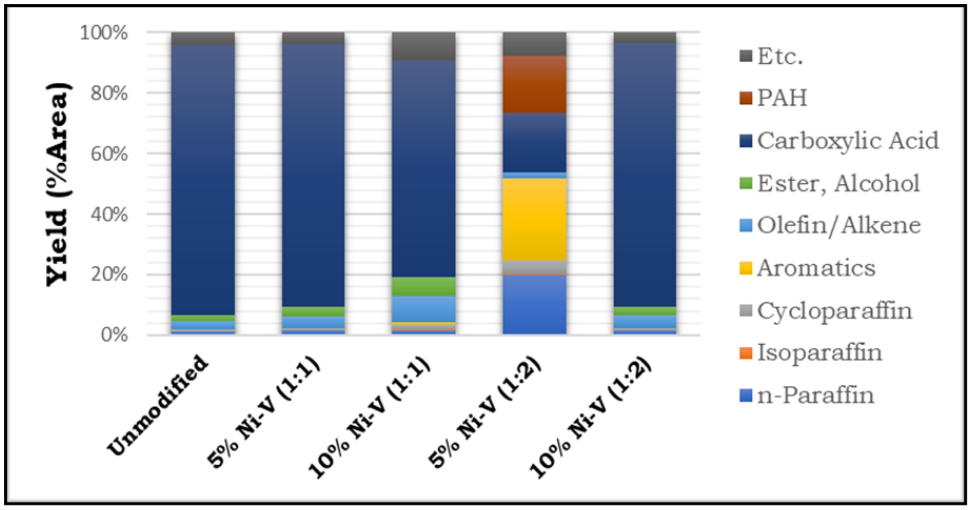

Figure 9. Distribution of components of the liquid product compound group of the hydrocracking reaction with variations in the HTs.

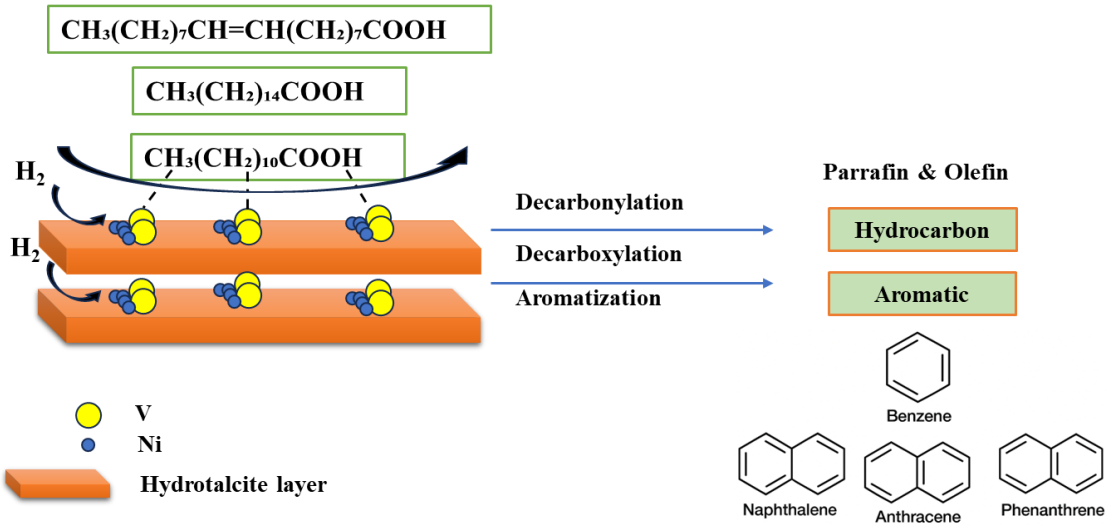

Figure 10. Simple purpose mechanism of the hydrocracking WCO using Ni-V/HTs catalyst.

Figure 11 presents the distribution of liquid fuel fractions obtained from catalytic activity tests using synthesized hydrotalcite (HTs) and its Ni–V modified forms. The unmodified hydrotalcite produced only kerosene (0.56%) and gasoil (1.49%), indicating low catalytic activity. Modification with Ni–V metals significantly altered the product distribution. The 5% Ni–V (1:2)/HTs catalyst achieved the highest liquid fuel yield, producing gasoline (1.69%), kerosene (13.72%), and gasoil (10.22%). This result demonstrates that the Ni: V ratio of 1:2 provides an optimal balance between hydrogenation (Ni) and redox (V) functions, thereby enhancing conversion efficiency [57]. In comparison, the 5% Ni–V (1:1)/HTs catalyst produced gasoline (1.92%), kerosene (0.33%), and gasoil (1.40%), but the total liquid fraction yield was lower than that obtained with the 1:2 ratio. Increasing the metal loading to 10% reduced catalytic activity. For 10% Ni–V (1:1)/HTs, only kerosene (0.24%) and gasoil (3.36%) were obtained, while 10% Ni–V (1:2)/HTs produced kerosene (0.43%) and gasoil (2.04%). These results indicate that excessive metal loading may block the active sites of the hydrotalcite support and hinder reactant diffusion, leading to lower conversion efficiency [19]. Overall, the 5% Ni–V (1:2)/HTs catalyst exhibited the best performance, with high selectivity toward

kerosene and gasoil fractions, which are particularly important for liquid biofuel applications [58].

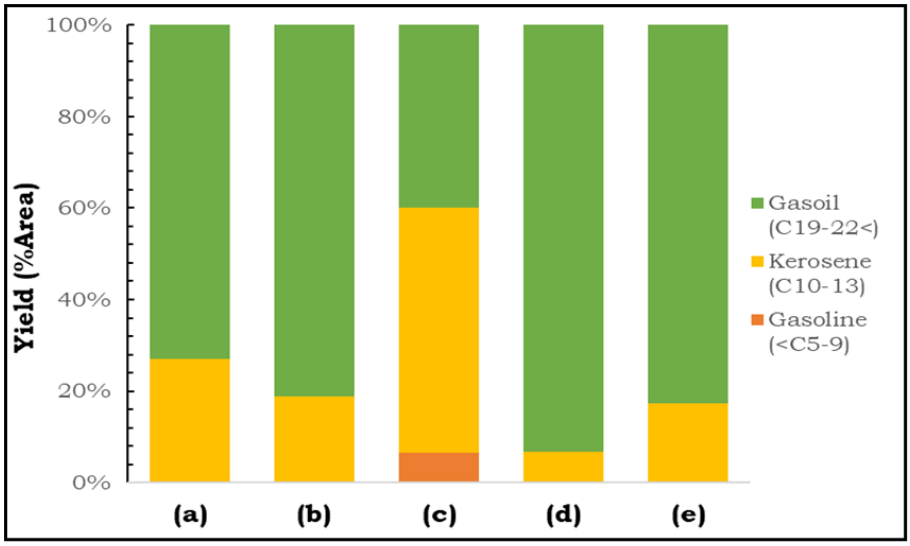

Figure 11. Fractions of liquid product components from catalytic activity tests using: **(a)** HTs; **(b)** 5% Ni-V (1:1)/HTs; **(c)** 5% Ni-V (1:2)/HTs; **(d)** 10% Ni-V (1:1)/HTs; **(e)** 10% Ni-V (1:2)/HTs.

4. Conclusions

The 5% Ni–V/HTs catalyst with a 1:2 metal ratio demonstrated the best performance compared to other catalyst formulations. Catalytic test results showed a significant reduction of carboxylic acids in WCO, from 94.02% to 19.79%. In addition, there was also a significant increase in the composition of hydrocarbons and aromatic compounds, reaching 26.69 and 45.59% respectively. The hydrocarbons in liquid products were predominantly composed of the kerosene fraction (C_{10}–C_{13},13.72%), followed by gasoil (C_{14}–C_{22}<, 10.22%). Notably, a gasoline fraction (<C_5–C_9, 1.69%) was also obtained, which was not detected in other catalyst modifications. These findings indicate that the 5% Ni–V (1:2)/HTs catalyst provides optimal activity and selectivity for liquid fuel production from WCO.

Author Contributions

Conceptualization, M.A.M., A.A.I.D. and L.M.; methodology, M.A.M.; software, A.A.I.D.; validation, S.S, and L.M.; formal analysis, S.P., R.E.N., and H.H.K.; investigation, M.P.M.; resources, M.P.M., M.A.M., and L.M; data curation, A.A., A.A.N., and H.P.; writing—original draft preparation, M.P.M., and M.A.M.; writing—review and editing, A.A; visualization, A.A.I.D; supervision, L.M., and M.A.M; project administration, M.A.M; funding acquisition, M.P.M., M.A.M., L.M., and S.P. All authors have read and agreed to the published version of the manuscript.

Institutional Review Board Statement

Not applicable.

Informed Consent Statement

Not applicable.

Data Availability Statement

Data supporting the findings of this study are available upon reasonable request from the corresponding author.

Funding

This research received no external funding.

Acknowledgments

This work was supported in part by the Research Organization for Nanotechnology and Materials – National Research and Innovation Agency (BRIN) research grant 2025. This work was also carried out with financial support from the PNBP Faculty of Science and Technology, under the Applied Research scheme at the University of Jambi, for the 2025 Fiscal Year. The authors acknowledge the facilities and scientific and technical support from Advanced Characterization Physics Laboratories Serpong, National Research and Innovation Agency, through E-Layanan Sains, Badan Riset dan Inovasi Nasional (BRIN).

Conflicts of Interest

The authors declare that they have no competing interests.

References

1. Lauermannová, A.-M.; Paterová, I.; Patera, J.; Skrbek, K.; Jankovský, O.; Bartůněk, V. Hydrotalcites in Construction Materials. *Appl. Sci.* **2020**, *10*, 7989, https://doi.org/10.3390/app10227989.
2. Wang, J.; Xiao, X.; Li, J.; Gao, X.; Zheng, J.; Chu, W. Hydrotalcite-derived Ni-LDO catalysts via new approach for enhanced performances in CO_2 catalytic reduction. *Fuel* **2022**, *324*, 124491, https://doi.org/10.1016/j.fuel.2022.124491.
3. Zhang, Y.; Li, Y.; Chen, J.; Xue, Z. Influence of magnesium-aluminum hydrotalcite on the microstructure and mechanical properties of magnesia castables. *Ceram. Int.* **2022**, *48*, 3923-3932, https://doi.org/10.1016/j.ceramint.2021.10.179.
4. Duan, W.; Li, G.; Wang, Z.; Wang, D.; Yu, Q.; Zhan, Y. Highly efficient production of hydrotalcite-like compounds from blast furnace slag. *Appl. Clay Sci.* **2022**, *219*, 106441, https://doi.org/10.1016/j.clay.2022.106441.
5. Exner, K.S.; Over, H. Kinetics of Electrocatalytic Reactions from First-Principles: A Critical Comparison with the Ab Initio Thermodynamics Approach. *Acc. Chem. Res.* **2017**, *50*, 1240–1247, https://doi.org/10.1021/acs.accounts.7b00077.
6. Mandari, V.; Devarai, S.K. Biodiesel Production Using Homogeneous, Heterogeneous, and Enzyme Catalysts via Transesterification and Esterification Reactions: a Critical Review. *Bioenergy Res.* **2022**, *15*, 935–961, https://doi.org/10.1007/s12155-021-10333-w.
7. Fanani, Z.; Asri, W.R.; Dwiyanti, B.; Rinaldi, N.; Maryana, R.; Al Muttaqii, M.; Riyanti, F.; Mara, A.; Zainul, R.; Hasanudin, H. Efficient Catalytic Hydrocracking of Crude Palm Oil Over EDTA Template-assisted SiO_2-Al_2O_3/NiMo Catalysts. *Period. Polytech. Chem. Eng.* **2024**, *68*, 552-560, https://doi.org/10.3311/PPch.37159.
8. Adany, F.; Priyanto, S.; Mirzayanti, Y.W.; Marbun, M.P.; Zainul Furqon, M.I.; Amin, A.K.; Hasanudin, H.; Aziz, A.; Nugraha, R.E.; Sudibyo, S.; Constan Lotebulo Ndruru, S.T.; Annas, D.; Yati, I.; Sulaswatty, A.; Khoiru Wihadi, M.N.; Wahyu N Nugroho, R.; Al Muttaqii, M. γ- Al_2O_3-supported Cobalt and Zinc as heterogeneous catalyst for biodiesel production assisted by ultrasonic wave. *Vacuum* **2025**, *240*, 114502, https://doi.org/10.1016/j.vacuum.2025.114502.
9. Jayaprakash, S.; Dewangan, N.; Jangam, A.; Das, S.; Kawi, S. LDH-derived Ni–MgO–Al_2O_3 catalysts for hydrogen-rich syngas production via steam reforming of biomass tar model: Effect of catalyst synthesis methods. *Int. J. Hydrog. Energy* **2021**, *46*, 18338-18352, https://doi.org/10.1016/j.ijhydene.2021.03.013.

10. Trujillano, R.; Rives, V.; Miguel, R.; González, B. Preparation of Original and Calcined Layered Double Hydroxide as Low-Cost Adsorbents: The Role of the Trivalent Cation on Methylene Blue Adsorption. *Molecules* **2023**, *28*, 4717, https://doi.org/10.3390/molecules28124717.
11. Zhang, Y.; Wang, J.; Chen, J.; Li, Y.; Xue, Z. Reconstruction and hydration of hydrotalcite response to thermal activation temperature: Enhancement of properties for magnesia castables. *Ceram. Int.* **2022**, *48*, 31245-31254, https://doi.org/10.1016/j.ceramint.2022.06.199.
12. Huang, J.; Xie, L.; Luo, X.; Wang, C.; Shu, R.; Song, Q.; Liu, J.; Tian, Z.; Chen, Y. Hydrogen production by aqueous phase reforming over stable La-promoted Ni-based hydrotalcite catalysts. *Int. J. Hydrog. Energy* **2024**, *50*, 681-689, https://doi.org/10.1016/j.ijhydene.2023.10.333.
13. Hasanudin, H.; Asri, W.R.; Mara, A.; Al Muttaqii, M.; Maryana, R.; Rinaldi, N.; Sagadevan, S.; Zhang, Q.; Fanani, Z.; Hadiah, F. Enhancement of Catalytic Activity on Crude Palm Oil Hydrocracking over SiO_2/Zr Assisted with Potassium Hydrogen Phthalate. *ACS Omega* **2023**, *8*, 20858-20868, https://doi.org/10.1021/acsomega.3c01569.
14. Jambhulkar, D.K.; Ugwekar, R.P.; Bhanvase, B.A.; Barai, D.P. A review on solid base heterogeneous catalysts: preparation, characterization and applications. *Chem. Eng. Commun.* **2022**, *209*, 433-484, https://doi.org/10.1080/00986445.2020.1864623.
15. Triyono; Trisunaryanti, W.; Purbonegoro, J.; Aksanti, S.I. Effect of cobalt impregnation methods on Parangtritis sand towards catalysts activity in hydrocracking of degummed low-quality Ujung Kulon Malapari oil into biohydrocarbons. *Reac. Kinet. Mech. Catal.* **2024**, *137*, 303-321, https://doi.org/10.1007/s11144-023-02538-1.
16. Zhang, X.; Dong, Y.; Cui, L.; An, D.; Feng, Y. Removal of Elemental Mercury from Coal Pyrolysis Gas Using Fe–Ce Oxides Supported on Lignite Semi-coke Modified by the Hydrothermal Impregnation Method. *Energy Fuels* **2018**, *32*, 12861-12870, https://doi.org/10.1021/acs.energyfuels.8b02358.
17. Madzaki, H.; Wan Ab Karim Ghani, W.A.; Yaw, T.C.S.; Rashid, U.; Muda, N. Carbon Dioxide Adsorption on Activated Carbon Hydrothermally Treated and Impregnated with Metal Oxides. *J. Kejuruter.* **2018**, *30*, 31–38, https://doi.org/10.17576/jkukm-2018-30(1)-05.
18. Aderibigbe, F.A.; Mustapha, S.I.; Adewoye, T.L.; Mohammed, I.A.; Gbadegesin, A.B.; Niyi, F.E.; Olowu, O.I.; Soretire, A.G.; Saka, H.B. Qualitative role of heterogeneous catalysts in biodiesel production from *Jatropha curcas* oil. *Biofuel Res. J.* **2020**, *7*, 1159-1169, https://doi.org/10.18331/BRJ2020.7.2.4.
19. Aziz, A.; Andini Putri, B.G.; Prasetyoko, D.; Nugraha, R.E.; Holilah, H.; Bahruji, H.; Jalil, A.A.; Suprapto, S.; Hartati, H.; Asikin-Mijan, N. Synthesis of mesoporous zeolite Y using *Sapindus rarak* extract as natural organic surfactant for deoxygenation of *Reutealis trisperma* oil to biofuel. *RSC Adv.* **2023**, *13*, 32648-32659, https://doi.org/10.1039/d3ra05390c.
20. Marlinda, L.; Prajitno, D.H.; Roesyadi, A.; Gunardi, I.; Mirzayanti, Y.W.; Al Muttaqii, M.; Budianto, A. Biofuel from hydrocracking of Cerbera manghas oil over Ni-Zn/HZSM-5 catalyst. *Eclética Química* **2022**, *47*, 17-39, https://doi.org/10.26850/1678-4618eqj.v47.1.2022.p17-39.
21. Aini, A.N.; Al-Muttaqii, M.; Roesyadi, A.; Kurniawansyah, F. Performance of Ni-Cu/HZSM-5 Catalyst in Hydrocracking Process to Produce Biofuel from *Cerbera manghas* Oil. *Key Eng. Mater.* **2021**, *884*, 149-156, https://doi.org/10.4028/www.scientific.net/KEM.884.149.
22. Al-Muttaqii, M.; Kurniawansyah, F.; Prajitno, D.H.; Roesyadi, A. Hydrocarbon Biofuel Production by Hydrocracking Process with Nickel-Iron Supported on HZSM-5 Catalyst. *IOP Conf. Ser.: Mater. Sci. Eng.* **2019**, *543*, 012055, https://doi.org/10.1088/1757-899X/543/1/012055.
23. Al Muttaqii, M.; Marbun, M.P.; Priyanto, S.; Sibuea, A.; Simanjuntak, W.; Syafaat Am, F.; Silalahi Raja, H.S.H.; Alviany, R.; Maryani, T.; Sulistyaningsih, T.; Prasetyo, E.; Sudibyo, S.; Yati, I. Lampung Natural Zeolite Dopped with of ZnO-TiO2 Metal Oxide as Catalyst for Biodiesel Production. *Bull. Chem. React. Eng. Catal.* **2024**, *19*, 61–68, https://doi.org/10.9767/bcrec.20038.
24. Pinthong, P.; Praserthdam, P.; Jongsomjit, B. Oxidative Dehydrogenation of Ethanol over Vanadium- and Molybdenum-modified Mg-Al Mixed Oxide Derived from Hydrotalcite. *J. Oleo Sci.* **2019**, *68*, 679-687, https://doi.org/10.5650/jos.ess19035.
25. Nazarova, G.; Ivashkina, E.; Ivanchina, E.; Oreshina, A.; Dolganova, I.; Pasyukova, M. Modeling of the catalytic cracking: Catalyst deactivation by coke and heavy metals. *Fuel Process. Technol.* **2020**, *200*, 106318, https://doi.org/10.1016/j.fuproc.2019.106318.
26. Świrk Da Costa, K.; Summa, P.; Wierzbicki, D.; Motak, M.; Da Costa, P. Vanadium promoted Ni(Mg,Al)O hydrotalcite-derived catalysts for CO_2 methanation. *Int. J. Hydrog. Energy* **2021**, *46*, 17776-17783, https://doi.org/10.1016/j.ijhydene.2021.02.172.

27. Summa, P.; Świrk, K.; Wierzbicki, D.; Motak, M.; Alxneit, I.; Rønning, M.; Da Costa, P. Co-Precipitated Ni-Mg-Al Hydrotalcite-Derived Catalyst Promoted with Vanadium for CO_2 Methanation. *Molecules* **2021**, *26*, 6506. https://doi.org/10.3390/molecules26216506.
28. Naghipour, A.; Ghorbani-Choghamarani, A.; Taherinia, Z. Novel hybrid materials based on mesoporous Gamma-Alumina@ Riboflavin@ vanadium for biodiesel production. *Fuel* **2023**, *334*, 126674, https://doi.org/10.1016/j.fuel.2022.126674.
29. Hafshah, H.; Prajitno, D.H.; Roesyadi, A. Hydrotalcite Catalyst for Hydrocracking Calophyllum inophyllum Oil to Biofuel: A Comparative Study with and without Nickel Impregnation. *Bull. Chem. React. Eng. Catal.* **2017**, *12*, 273–280, https://doi.org/10.9767/bcrec.12.2.776.273-280.
30. Arhzaf, S.; Bennani, M.N.; Abouarnadasse, S.; Ziyat, H.; Qabaqous, O. Effect of Mg/Al molar ratio on the basicity of Mg-Al mixed oxide derived from Mg-Al hydrotalcite. *Mediterr. J. Chem.* **2020**, *10*, 625-633, https://doi.org/10.13171/mjc10602007021464sa.
31. Utami, M.; Trisunaryanti, W.; Shida, K.; Tsushida, M.; Kawakita, H.; Ohto, K.; Wijaya, K.; Tominaga, M. Hydrothermal preparation of a platinum-loaded sulphated nanozirconia catalyst for the effective conversion of waste low density polyethylene into gasoline-range hydrocarbons. *RSC Adv.* **2019**, *9*, 41392-41401, https://doi.org/10.1039/c9ra08834b.
32. Muttaqii, M.A.; Annas, D.; Yati, I.; Kurniawan, H.H.; Ndruru, S.T.C.L.; Priyanto, S.; Sudibyo; Aziz, A.; Prasetyoko, D.; Nugraha, R.E.; Marlinda, L. Molybdenum-lanthanum supported on nano-HZSM-5 as catalyst for hydroprocessing of *Cerbera manghas* oil. *Inorg. Chem. Commun.* **2025**, *173*, 113855, https://doi.org/10.1016/j.inoche.2024.113855.
33. Du, Y.; Huang, C.; Jiang, W.; Yan, Q.; Li, Y.; Chen, G. Preparation of surface modified nano-hydrotalcite and its applicaiton as a flow improver for crude oil. *Fuel* **2024**, *357*, 130005, https://doi.org/10.1016/j.fuel.2023.130005.
34. Wang, S.; Zheng, Y.; Lang, M. Preparation of Hydrotalcite/SBA-15 Composite Catalyst and its Application in the Synthesis of ε-Caprolactone. *Catal. Lett.* **2024**, *154*, 6094-6105, https://doi.org/10.1007/s10562-024-04763-2.
35. Muttaqii, M.A.; Kurniawansyah, F.; Prajitno, D.H.; Roesyadi, A. Hydrocracking process of coconut oil using Ni-Zn/HZSM-5 catalyst for hydrocarbon biofuel production. *J. Phys.: Conf. Ser.* **2021**, *1725*, 012008, https://doi.org/10.1088/1742-6596/1725/1/012008.
36. Ma, R.; Du, Y.; Liu, X.; Liu, J.; Wu, X. Synthesis of a novel CoNiV mixed oxides from hydrotalcite precursor and its application for selective catalytic oxidation of slip ammonia. *J. Energy Inst.* **2022**, *102*, 327-336, https://doi.org/10.1016/j.joei.2022.04.004.
37. Xiong, L.; Qiu, Y.; Dong, H.; Gao, B.; Zhang, X.; Chu, P.K.; Peng, X. Metallic Ni_3N/Ni heterostructure for efficient hydrogen evolution reaction. *Int. J. Hydrogen Energy* **2024**, *59*, 400-407, https://doi.org/10.1016/j.ijhydene.2024.01.312.
38. Zhang, H.; Gao, X.; Yao, F.; Yue, H. Controllable synthesis of vanadium-doped nickel-chalcogenide/graphene cathodes and $MnV_2O_6{\cdot}2H_2O$/graphene anode for high-energy asymmetric supercapacitors. *J. Energy Storage* **2023**, *61*, 106717, https://doi.org/10.1016/j.est.2023.106717.
39. Paras; Yadav, K.; Kumar, P.; Teja, D.R.; Chakraborty, S.; Chakraborty, M.; Mohapatra, S.S.; Sahoo, A.; Chou, M.M.C.; Liang, C.-T.; Hang, D.-R. A Review on Low-Dimensional Nanomaterials: Nanofabrication, Characterization and Applications. *Nanomaterials* **2023**, *13*, 160, https://doi.org/10.3390/nano13010160.
40. Mališová, M.; Horňáček, M.; Hudec, P.; Mikulec, J.; Jorík, V.; Hájeková, E. Influence of hydrotalcite preparation conditions on its physico-chemical properties. *Acta Chim. Slov.* **2019**, *12*, 119-126, https://doi.org/10.2478/acs-2019-0017.
41. Park, S.; Kwon, D.; Kang, J.Y.; Jung, J.C. Influence of the preparation method on the catalytic activity of MgAl hydrotalcites as solid base catalysts. *Green Energy Environ.* **2019**, *4*, 287-292, https://doi.org/10.1016/j.gee.2018.11.003.
42. Ambroz, F.; Macdonald, T.J.; Martis, V.; Parkin, I.P. Evaluation of the BET Theory for the Characterization of Meso and Microporous MOFs. *Small Methods* **2018**, *2*, 1800173, https://doi.org/10.1002/smtd.201800173.
43. Aziz, A.; Nugraha, R.E.; Holilah, H.; Bahruji, H.; Al Muttaqii, M.; Suprapto, S.; Prasetyoko, D. Hydrothermal study of synthesis mesoporous NaP zeolite using *Sapindus rarak* extract as natural surfactant. *Inorg. Chem. Commun.* **2024**, *165*, 112497, https://doi.org/10.1016/j.inoche.2024.112497.
44. Parkash, A. Doping of Fe on room-temperature-synthesized CoNi layered double hydroxide as an excellent bifunctional catalyst in alkaline media. *J. Iran. Chem. Soc.* **2020**, *17*, 2943–2956,

https://doi.org/10.1007/s13738-020-01970-7.
45. Seekhiaw, P.; Jantasee, S.; Praserthdam, P.; Jongsomjit, B. Effect of Strontium Modification in Mg–Al Mixed Oxide Catalysts on Product Distribution toward Catalytic Reaction of Ethanol. *ACS Omega* **2023**, *8*, 32775-32783, https://doi.org/10.1021/acsomega.3c03752.
46. Pan, S.; Zha, M.; Gao, C.; Qu, J.; Ding, X. Pore Structure and Fractal Characteristics of Organic-Rich Lacustrine Shales of the Kongdian Formation, Cangdong Sag, Bohai Bay Basin. *Front. Earth Sci.* **2021**, *9*, 760583, https://doi.org/10.3389/feart.2021.760583.
47. Cui, C.; Ma, J.; Wang, Z.; Liu, W.; Liu, W.; Wang, L. High Performance of Mn-Doped $MgAlO_x$ Mixed Oxides for Low Temperature NO_x Storage and Release. *Catalysts* **2019**, *9*, 677, https://doi.org/10.3390/catal9080677.
48. Lu, B.; Zhuang, J.; Du, J.; Gu, F.; Xu, G.; Zhong, Z.; Liu, Q.; Su, F. Highly Dispersed Ni Nanocatalysts Derived from NiMnAl-Hydrotalcites as High-Performing Catalyst for Low-Temperature Syngas Methanation. *Catalysts* **2019**, *9*, 282, https://doi.org/10.3390/catal9030282.
49. Suzihaque, M.U.H.; Alwi, H.; Kalthum Ibrahim, U.; Abdullah, S.; Haron, N. Biodiesel production from waste cooking oil: A brief review. *Mater. Today: Proc.* **2022**, *63*, S490-S495, https://doi.org/10.1016/j.matpr.2022.04.527.
50. Shi, X.; Wang, K.; Wang, M.; Yuan, H. Oleic acid decarboxylation to produce C_8-C_{17} alkanes catalyzed by Pt and Ni on a MOF-derived zirconia. *J. Porous Mater.* **2024**, *31*, 2275-2289, https://doi.org/10.1007/s10934-024-01676-8.
51. Al Muttaqii, M.; Marbun, M.P.; Sudibyo, S.; Aunillah, A.; Pranowo, D.; Hasanudin, H.; Rinaldi, N.; Bardant, T.B. Conversion of Sunan Candlenut Oil to Aromatic Hydrocarbons with Hydrocracking Process Over Nano-HZSM-5 Catalyst. *Bull. Chem. React. Eng. Catal.* **2024**, *19*, 141–148, https://doi.org/10.9767/bcrec.20116.
52. Sekar, M.; T R, P. Critical review on the formations and exposure of polycyclic aromatic hydrocarbons (PAHs) in the conventional hydrocarbon-based fuels: Prevention and control strategies. *Chemosphere* **2024**, *350*, 141005, https://doi.org/10.1016/j.chemosphere.2023.141005.
53. Yilmaz, N.; Vigil, F.M.; Donaldson, B. Fuel effects on PAH formation, toxicity and regulated pollutants: Detailed comparison of biodiesel blends with propanol, butanol and pentanol. *Sci. Total Environ.* **2022**, *849*, 157839, https://doi.org/10.1016/j.scitotenv.2022.157839.
54. Vu, X.H.; Nguyen, S.; Dang, T.T.; Armbruster, U. Improved biofuel quality in catalytic cracking of triglyceride-rich biomass over nanocrystalline and hierarchical ZSM-5 catalysts. *Biomass Conv. Bioref.* **2021**, *11*, 755-766, https://doi.org/10.1007/s13399-020-00713-1.
55. Marlinda, L.; Aziz, A.; Roesyadi, A.; Prajitno, D.H.; Mirzayanti, Y.W.; Al-Muttaqii, M. Cobalt-nickel supported on desilicated HZSM-5 for the conversion of Reutealis trisperma (blanco) airy shaw oil to liquid hydrocarbon products. *Commun. Sci. Technol.* **2025**, *10*, 87-97, https://doi.org/10.21924/cst.10.1.2025.1570.
56. Marlinda, L.; Al-Muttaqii, M.; Roesyadi, A.; Danawati, H.P. Production of biofuel by hydrocracking of *cerbera manghas* oil using Co-Ni/HZSM-5 catalyst: Effect of reaction temperature. *J. Pure App. Chem. Res* **2016**, *5*, 189-195, https://doi.org/10.21776/ub.jpacr.2016.005.03.254.
57. Choi, D.S.; Kim, N.Y.; Yoo, E.; Kim, J.; Joo, J.B. Enhanced coke resistant $Ni/SiO_2@SiO_2$ core–shell nanostructured catalysts for dry reforming of methane: Effect of metal-support interaction and SiO_2 shell. *Chem. Eng. Sci.* **2024**, *299*, 120480, https://doi.org/10.1016/j.ces.2024.120480.
58. Marlinda, L.; Priyanto, S.; Oktiarmi, P.; Marbun, M.P.; Dewi, A.A.I.; Sudibyo, S.; Yati, I.; Aziz, A.; Nugraha, R.E.; Al Muttaqii, M. Nickel-vanadium impregnated to hydrotalcite for hydrocracking of waste cooking oil. *Int. J. Renew. Energy Dev.* **2026**, *15*, 464–473, https://doi.org/10.61435/ijred.2026.61972.

Publisher's Note & Disclaimer

information before relying on it, and the publisher assumes no responsibility for any consequences arising from the use of materials contained in this publication.